IOP PUBLISHING PLASMA PHYSICS AND CONTROLLED FUSION

Plasma Phys. Control. Fusion **49** (2007) B419–B427 doi:10.1088/0741-3335/49/12B/S39

Thin film deposition by means of atmospheric pressure microplasma jet

J Benedikt, V Raballand, A Yanguas-Gil, K Focke and A von Keudell

Arbeitsgruppe Reaktive Plasmen, Fakultät für Physik und Astronomie, Ruhr-Universität Bochum, Universitätsstr. 150, 44780 Bochum, Germany

Received 6 July 2007
Published 19 November 2007
Online at stacks.iop.org/PPCF/49/B419

Abstract

An RF microplasma jet working at atmospheric pressure has been developed for thin film deposition application. It consists of a capillary coaxially inserted in the ceramic tube. The capillary is excited by an RF frequency of 13.56 MHz at rms voltages of around 200–250 V. The plasma is generated in a plasma forming gas (helium or argon) in the annular space between the capillary and the ceramic tube. By adjusting the flows, the flow pattern prevents the deposition inside the source and mixing of the reactive species with the ambient air in the discharge and deposition region, so that no traces of air are found even when the microplasma is operated in an air atmosphere. All these properties make our microplasma design of great interest for applications such as thin film growth or surface treatment. The discharge operates probably in a γ-mode as indicated by high electron densities of around 8×10^{20} m^{-3} measured using optical emission spectroscopy. The gas temperature stays below 400 K and is close to room temperature in the deposition region in the case of argon plasma. Deposition of hydrogenated amorphous carbon films and silicon oxide films has been tested using Ar/C_2H_2 and Ar/hexamethyldisiloxane/O_2 mixtures, respectively. In the latter case, good control of the film properties by adjusting the source parameters has been achieved with the possibility of depositing carbon free SiO_x films even without the addition of oxygen. Preliminary results regarding permeation barrier properties of deposited films are also given.

1. Introduction

Atmospheric pressure microplasma discharges have attracted a great deal of attention due to their interesting properties such as high electron density inaccessible for typical low pressure plasmas (n_e up to 10^{21} m^{-3}) and very low gas temperatures (T_g as small as 300 K). Moreover, operation at atmospheric pressure and low power consumption ($\leqslant$1 W) make them attractive for on-chip implementation and mass production. Up to now, a number of different configurations have been described in the literature for microplasmas operated at atmospheric pressure. Examples are microhollow cathode discharges, capillary plasma

electrode discharges, cylindrical dielectric barrier discharges, miniature inductively and capacitively coupled plasmas, jets or devices fabricated in semiconductor structures. Becker *et al* [1] and Foest *et al* [2] review some of the most common configurations. Microplasma sources can be dc, RF or MW driven and they can be used for example as photonic devices [3,4], as analytical tools [5], for bacterial inactivation [6] or for etching of silicon wafers [7]. However, the large surface to volume ratio and the miniature size make it difficult to use these microplasmas with reactive gases for coating applications. The deposition or erosion of electrodes results in the fast deterioration of the microplasma source performance. Moreover, the transport of reactive species from the plasma to the treated surface is more complex than in the low pressure discharges, since diffusion is slow and three body recombination reactions as well as frequent collisions lead to the fast quenching of reactive species. Only a few deposition systems based on microplasma jets have been reported [8–10], in which the fast convection assures the transport of reactive species to the film surface. Any successful deposition of good quality material using a microplasma device would open a new window of opportunities such as *in vivo* deposition or repair of bio-compatible films, local deposition of, e.g. dielectric barriers at atmospheric pressure or coating of nanoparticles, when injected with the precursor gas into the plasma.

The goal of this paper is to discuss the main aspects and critical issues involved in thin film deposition by means of atmospheric pressure microplasma jets and to provide some strategies useful in a design of new microplasma jet based depositing tools. As an example, an RF microplasma jet source optimized for thin film deposition applications is presented. The paper is organized in the following way: first the experimental setup and diagnostic techniques are described. Second, the issues relevant to the plasma source operation, such as gas mixing or influence of an ambient atmosphere, are discussed. Afterwards, the results for helium and argon plasma without reactive gas are presented and discussed. Finally, the properties of thin films deposited using acetylene and organosilicon precursor are summarized.

2. Experimental setup

The scheme of our microplasma jet is shown in figure 1. A stainless steel capillary with outer and inner diameters of 0.5 and 0.2 mm is inserted into a ceramic tube (Degussit De-23, $\varepsilon_r = 9.8$) with an inner diameter of 1 mm. A gap of 250 μm is formed between the capillary and the tube in this way. The capillary ends 2 mm prior to the end of the ceramic tube. On the outside of the ceramic tube (outer diameter 1.5 mm) an 8 mm long aluminium tube serves as a grounded electrode. The edge of this tube is placed 1 mm apart from the end of the ceramic tube. The capillary is connected to a 13.56 MHz power supply through a matching network. The ceramic tube holder, capillary mount and gas and power lines are all built in a plastic body (POM material) which is mounted on a 40 mm ISO-KF flange. The microplasma jet is mounted on a small chamber (volume 3 L) allowing the control of the ambient atmosphere, but it can be hand-held operated. Argon or helium serve as a plasma forming gas. Plasma forming gas is guided into the plasma source through the annular space between the ceramic tube and the capillary (*main flow*). The precursor gas is injected into the plasma plume, formed at the exit of the source, through the capillary (*capillary flow*) (see figure 1). Both the *main flow* and the *capillary flow* are controlled by mass flow controllers. We have tested oxygen (O_2), nitrogen (N_2), hydrogen (H_2) methane (CH_4), acetylene (C_2H_2), tetramethylsilane (TMS), hexamethyldisiloxane (HMDSO) or their combinations as precursor gases up to now. For the liquid precursors (TMS, HMDSO) a home-made bubbler with a controlled flow of argon has been constructed and operated at room temperature.

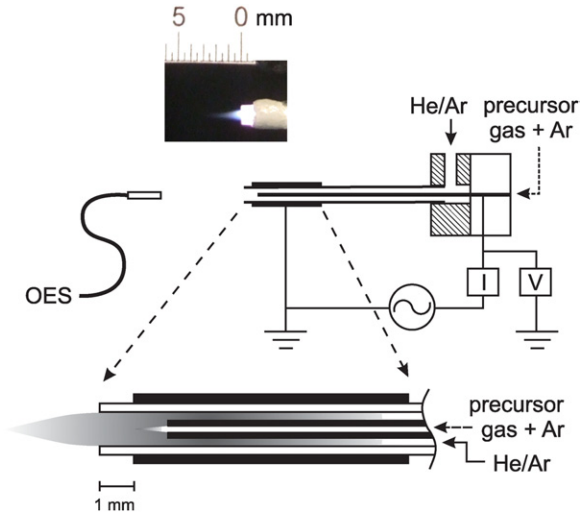

Figure 1. Scheme of the experimental setup together with the photograph of an argon microplasma jet.

The experimental arrangement is similar to the atmospheric pressure glow discharge torch presented by Léveillé and Coulombe [11], where helium is used as a plasma forming gas and oxygen as a precursor gas. However, the plasma jet presented here does not possess a pinched nozzle and an optimized flow with minimum shear between the gas flows through the capillary and the ceramic tube is maintained.

The discharge has been characterized by optical emission spectroscopy and by using voltage and current probes. Two spectrometers have been used: full spectra ranging from 200 to 900 nm have been obtained using a low resolution USB 2000 spectrometer from Ocean Optics with a resolution of 1.5 nm. Detailed measurements of band and line profiles have been carried out using a SpectraPro 500i spectrometer from Acton and a Princeton Instruments CCD camera, with a total resolution of 0.4 Å. In both cases the light is collected using an optical fibre with a collimating lens, which is placed on the axis 140 mm from the end of the microplasma jet (see figure 1). Current and voltage waveforms are measured with voltage and current probes (Tektronix P5100 and CT2, respectively) placed as shown in figure 1. The phase shift between the probes has been calibrated by the measurement of a 50 Ω dummy load. Deposited films are analyzed by means of a Fourier transform infrared spectrometer (FTIR, Bruker IFS 66), profilometer (Dektak 6M) and an atomic force microscope (Veeco CPII). Additionally, the oxygen permeation rate is determined by a MOCON OX-TRAN 2/61 instrument (MOCON Inc., Minneapolis) for the SiO_x films.

3. Results and discussion

3.1. Plasma operation

Helium and argon are used as plasma forming gases. Significant differences are observed between helium- and argon- operated plasmas. Discharges in He are ignited easily and the plasma fills the annular space between the capillary and the ceramic tube. Moreover, no visible jet appears at the end of the source. In contrast, argon microplasma is difficult to ignite, the

discharge is concentrated at the tip of the capillary and a visible jet, few millimetres long, is formed at the source exit as shown in figure 1. This distinct behavior is probably due to the different breakdown fields for these two gases. Paschen curves obtained experimentally by Moravej *et al* show that in our pd range the breakdown voltage is up to five times higher for Ar than for He [12]. The plasma is always ignited in He and only after that the gas flow is switched to argon in the case of argon plasma. The location of the argon plasma at the capillary tip is also the consequence of high breakdown voltage of argon. In our experimental set-up, the electric field inside the coaxial structure is not high enough to cause the breakdown in argon, and therefore no discharge is generated in that region. However, an enhancement of the electric field at the capillary tip is expected, so that the electric field strength can be higher than the breakdown electric field for Ar in this region and the plasma can be maintained there. This has been proven by electrostatic simulations without the plasma, which shows that the magnitude of the electric field close to the end of the inner capillary can be due to the field enhancement up to one order of magnitude higher than that inside the coaxial structure [13]. Both He and Ar are used to study the plasma parameters; however, the depositions are performed only with Ar as a plasma forming gas since He is due to its high price not acceptable for possible industrial application.

The flow conditions inside the source are critical for the source performance with respect to thin film deposition. If only a small flow of a precursor gas is injected through the capillary, the hydrodynamic velocity of *capillary flow* is several times smaller than the one of the *main flow* of argon. The shear between these two flows results in the formation of vortexes inside a tube, which results in a long residence time of the reactive species inside the source causing dust particle formation, inhomogeneous film growth and deposition inside the source, hence reducing its lifetime. When the hydrodynamic velocity of the *capillary flow* is enhanced by an admixture of argon, the shear stress between the two flows can be minimized without the formation of vortexes at the capillary tip. This can be demonstrated by simulating the laminar gas flow inside the source using the incompressible Navier–Stokes equation for argon at room temperature. The resulting velocity field and flow streamlines for the case of low *capillary flow* of only 25 sccm (hydrodynamic velocity of gas in the capillary is $15\,\mathrm{m\,s^{-1}}$) and optimized flow of 160 sccm (hydrodynamic velocity $93\,\mathrm{m\,s^{-1}}$) are shown in figure 2(*a*) and (*b*), respectively. The argon *main flow* is kept at 3 slm (hydrodynamic velocity in the annular space is $93\,\mathrm{m\,s^{-1}}$). The simulation clearly shows the formation of a vortex with very long residence time of the species just at the capillary end under not-optimized flow conditions. The simulation results presented in figure 2 are only an approximation of a real case, since the flow inside the source is in the transient stage between laminar and turbulent conditions; however the experimental observations confirm that optimized flow conditions significantly improve the source performance and its lifetime [14]. In the following, the *capillary flow* is always optimized by the addition of an appropriate argon flow to the precursor flow.

An other issue connected with the source operation at atmospheric pressure is the influence of the ambient atmosphere on the plasma and deposited film properties. If air is the ambient atmosphere, nitrogen and oxygen might be admixed into the plasma and be incorporated into the film. However, in the presented source geometry, no N_2 or O_2 related emission was observed by OES. It indicates that the high flow of Ar creates a protective atmosphere around the jet, which prevents the ambient air from reaching the plasma. Adding 0.1% of N_2 to the total flow results however in a very strong emission of the second positive system of nitrogen [13]. The formation of a protective atmosphere in the emerging plasma jet has also been observed by Niemi *et al* [15], where the penetration of VUV radiation through the carrier gas atmosphere over a distance of several centimetres away from the atmospheric pressure

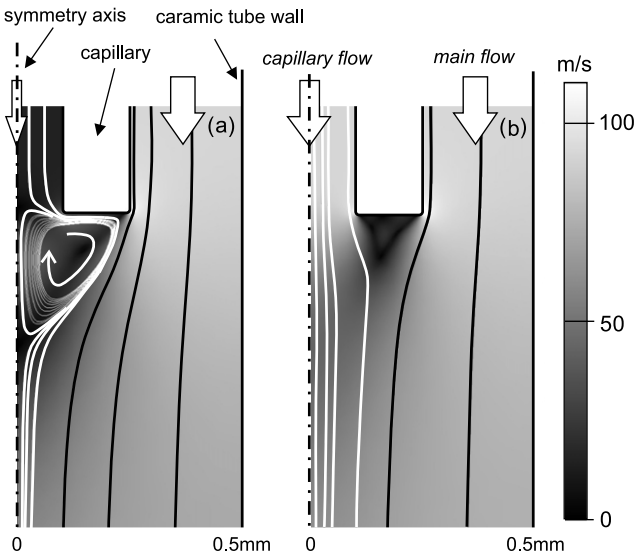

Figure 2. Laminar flow simulation of argon using incompressible Navier–Stokes equations. The velocity field (gray scale) and streamlines in the region of the capillary end are shown for the case with low hydrodynamic gas velocity (capillary flow 25 sccm, (*a*)) and optimized hydrodynamic gas velocity (capillary flow 160 sccm, (*b*)) in the capillary. Argon *main flow* is 3 slm with gas velocity in the annular space of 93 m s^{-1}.

plasma jet nozzle was observed. The presence of a protective atmosphere is also confirmed by the FTIR measurements of deposited a-C : H films [14].

The examples mentioned in this section demonstrate that the control of the flow is a crucial issue in the deposition application of any jet-like microplasma source.

3.2. Electrical and optical characterization

Discharges in He, Ar and Ar/CH_4, Ar/C_2H_2 mixtures have been characterized using current and voltage probes. If no plasma is running, the phase shift between the voltage and current is -88.45°, very close to the -90° phase shift of a perfect capacitor. The real part of the impedance of the complete source is $R = 13\,\Omega$ and the imaginary part is $477\,\Omega$. It should be noted that the measured impedance also includes the voltage probe impedance and the impedance of the electrical connections, which are larger than the impedance of the coaxial structure of the source with an estimated capacity of 0.6 pF. Without the plasma ignited, the voltage increases linearly with current and the absorbed power follows $I_{\mathrm{rms}}^2 R$ values as shown in figure 3. The same figure shows the rms voltage and absorbed power for the helium plasma (He flow 1.4 slm) as a function of rms current. He plasma ignites at an rms current of 0.2 A and an rms voltage of 95 V. No change in the absorbed power is observed due to the very small plasma volume and low plasma density. When observed from the front, a homogeneous plasma completely fills the annular space between the capillary and the ceramic tube. The discharge can be maintained after ignition at lower than breakdown voltages: a hysteresis is observed as indicated in figure 3. No additional power absorbed by the plasma is however measured up to approximately 0.28 A and 140 V. When the rms voltage is increased even further, a bright

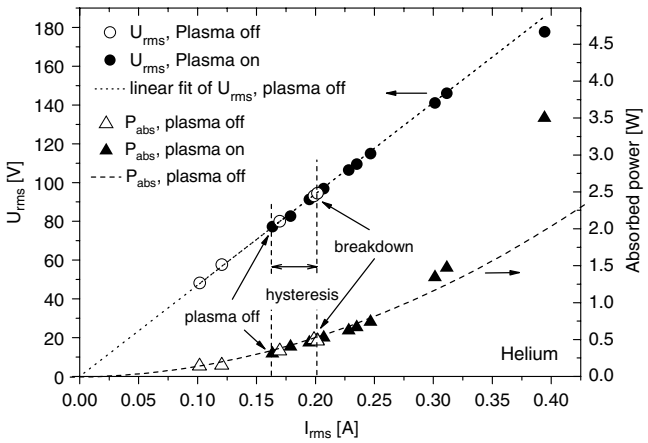

Figure 3. Rms voltage and absorbed power as a function of the rms current of an He microplasma. Helium flow is 1.4 slm.

region appears at the capillary surface and power absorbed by the plasma starts to be visible in figure 3. Yang *et al* [16] have studied an RF atmospheric pressure helium discharge in a parallel plate reactor and have reported an increase in electron density, an increase of power absorption and a localization of the discharge at the electrode surface when a sheath breakdown and a transition from the α- to the γ-mode discharge occur. We presume that the transition from the α- to the γ-mode discharge with an abrupt increase in electron density in the region close to the capillary can explain the observed behaviour of our microplasma in helium. This assumption is supported by relatively high electron density of $8.5 \times 10^{14}\,\mathrm{cm}^{-3}$ (as reported later in this paper). It is difficult to observe this transition for argon plasma; it has to be ignited with the help of helium and is concentrated only at the tip of the capillary, but since the plasma densities are similar for both gases we expect that the argon plasma is in the γ-mode as well.

The OES is used to determine the gas temperature and the electron density in both helium and argon microplasmas. A detailed description of the measurement procedure and data evaluation is given elsewhere and only a brief summary is given here [13]. The gas temperature has been determined from the analysis of the fine structure of the rotational bands of OH at 306 nm, assuming an equilibrium between the rotational and the translational degrees of freedom in the plasma, which is usually valid in atmospheric pressure discharges [17]. This OH emission originates from the fragmentation of water molecules that desorb from the ceramic tube. The temperatures are always around 350 ± 50 K regardless of the chosen power and gases. The low gas temperature has been corroborated by thermocouple measurements at a 3 mm distance from the end of the coaxial structure for different incident RF powers for Ar and He discharges. The temperature remains in both cases between room temperature and 350 K. The temperature is independent of the power used for Ar, whereas in the case of He the temperature is slightly higher and increases with power [13]. The enhanced gas temperature of the gas outside the source in the case of helium is probably due to higher discharge volume. Since the argon plasma is concentrated only at the capillary tip, only a small fraction of the gas is heated and the gas temperature is less sensitive to incident power.

The electron density has been determined using the Stark broadening of the H_β line in Ar and He mixtures and the complete procedure we used has been published elsewhere [13]. The electron density values of $8.5 \times 10^{14}\,\mathrm{cm}^{-3}$ and $7.0 \times 10^{14}\,\mathrm{cm}^{-3}$ are obtained for Ar and He plasmas, respectively. These densities are independent of the absorbed power for both

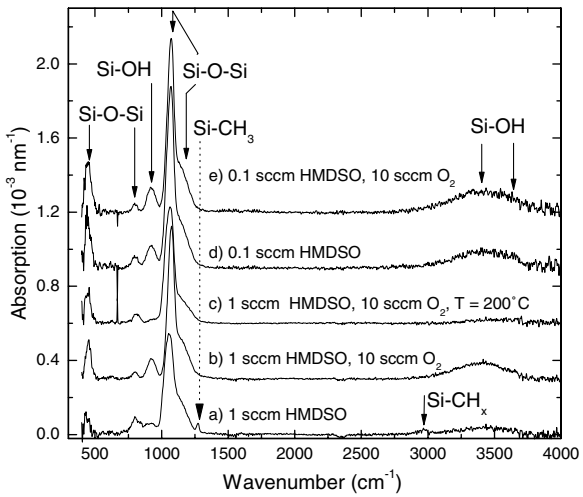

Figure 4. FTIR spectra for five different conditions with HMDSO flow and O_2 flow as indicated in the figure. Where not given, the substrate temperature is room temperature. Argon flow is 3 slm, capillary flow 160 sccm and rms voltage 205 V.

He and Ar discharges. In the case of Ar/CH_4 and Ar/C_2H_2 mixtures it was not possible to obtain electron densities from the H_β line profile due to the overlap of the atomic line with the molecular bands of C_2 species. The measured electron density in the range of $10^{15}\,\mathrm{cm}^{-3}$ is three orders of magnitude higher than electron densities reported for the α-mode atmospheric pressure helium discharge [18] or for the plasma needle [19]. This observation corroborates our assumption that the discharge operates in a γ-mode. The constant value of the electron density with increasing power is consistent with this assumption since the increase in power causes an increase in the discharge area at the electrode rather than an increase in electron density. This is also in agreement with our experience, as the size of the plume and the plasma region inside the coaxial structure increases with the dissipated power.

3.3. Film deposition and film properties

Thin films have been deposited from Ar/C_2H_2, Ar/TMS/O_2 and Ar/HMDSO/O_2 mixtures. First, the deposition of a-C : H films is briefly discussed. Typical FTIR spectra for a-C : H films deposited from the Ar/C_2H_2 mixture (C_2H_2 flow 1 to 30 sccm) have been published elsewhere [14]. The deposited films are soft, porous with polymer-like structure and with C=O bonds as a result of postoxidation after the deposition. The FTIR spectra are almost independent of the C_2H_2 flow and the applied power. This behaviour and low film quality are an expected result, since energetic ion bombardment of a growing film is the main factor controlling the film quality, and it is prevented by collisions at atmospheric pressure. The absence of energetic ion bombardment is a drawback of the atmospheric pressure deposition processes, which limits their application range to systems where ion bombardment does not play an important role. Better control of film properties can be achieved in the deposition of SiO_x films using organosilicon precursors such as TMS or HMDSO with an additional admixture of O_2. Figure 4 shows FTIR spectra of five SiO_x films deposited under various HMDSO and O_2 flows and at two different temperatures. The plasma parameters (argon *main flow* 3 slm, rms voltage 206 V, absorbed power 5 W) are kept constant and the distance

between the end of the source and the substrate is 1 mm. The absorptions due to Si–O–Si bond rocking, bending and stretching are visible around 400, 800, 1060 and 1160 cm^{-1} in all spectra. Additionally, absorptions due to the presence of carbon can appear at 850, 1265 and 2960 cm^{-1} and due to the OH groups at 920 cm^{-1} and broad bands around 3400 and 3650 cm^{-1}. The overview of the position and origin of possible absorption lines can be found elsewhere [20]. The deposited films contain carbon when a high HMDSO flow of 1 sccm is used and no oxygen is added (conditions (a) in figure 4). The HMDSO density in the source is much higher than the measured plasma (electron) density in this case. Reducing the HMDSO flow to 0.1 sccm or adding oxygen to the *capillary flow* results in carbon-free deposition (conditions (*b*), (*d*) and (*e*) in figure 4). However, the resulting material is probably porous as indicated by a rather high content of OH in the film and also by large absorption at the asymmetric stretching of Si–O–Si at 1160 cm^{-1} [21, 22]. The film quality can be further improved, when elevated substrate temperature is used, as shown in the FTIR spectrum (c) in figure 4. The OH absorption disappears under these conditions and the asymmetric stretching absorption at 1160 cm^{-1} is smaller relative to the absorption at 1060 cm^{-1}. The improved film quality at elevated temperature has been observed by Creatore *et al* [23] at low pressure remote deposition of SiO_x films or by Babayan *et al* [24] under atmospheric pressure conditions. The deposition rate on the source axis is in the range of 1 to 2 nm s^{-1} and the films are deposited typically on a few mm^2 area. The conversion efficiency of the precursor into the deposited film is approximately 1%, as calculated from the HMDSO flow, deposited volume and taking the SiO_2 density of 2.2 g cm^{-3}. The films are smooth with the roughness being under the 1.5 nm limit of our AFM. In order to test whether carbon-free SiO_x material deposited at room temperature (deposition (*e*)) can serve as a permeation barrier coating on polyethylene terephthalate (PET), a deposition of a 60 nm thick film has been realized on 1 cm^2 and the O_2 permeation has been compared with the permeation through PET foil without any deposition. A small 11% reduction of the O_2 permeation flux has been achieved. The permeation barrier properties are improved (25% reduction) when higher absorbed power (10 W), higher oxygen flow (50 sccm) and a 30 nm intermediate carbon containing layer (conditions (*a*)) are used. Additional experiments will be performed to test whether the barrier properties can be further improved.

4. Conclusions

The successful design and reliable operation of a microplasma jet source have been demonstrated. The design of the microplasma source, with the insertion of the reactive gases through a capillary inner electrode, the remote plasma generation and flow pattern control through the optimized flow prevents deposition inside the source, does not limit the selection of a precursor gas and shields the microplasma jet from the ambient atmosphere. These properties make our microplasma jet of great interest for applications such as thin film growth or surface treatment. The experimental characterization of the microplasma jet source shows that it operates probably in a γ-mode with high electron densities (8.5×10^{20} m^{-3} for Ar and 7.0×10^{20} m^{-3} for He discharges) and low gas temperatures (less than 400 K). Deposition of hydrogenated amorphous carbon films and silicon oxide films has been tested using Ar/C_2H_2 and Ar/hexamethyldisiloxane/O_2 mixtures, respectively. Good control of the film properties by adjusting the source parameters has been achieved in SiO_x deposition with the possibility of depositing carbon-free SiO_x films even without the addition of molecular oxygen. The film growth rate is in the 1–2 nm s^{-1} range with 1% conversion efficiency. The preliminary measurements of SiO_x films show only limited permeation barrier properties.

Acknowledgments

The authors thank Norbert Grabkowski for his skillful technical assistance and Michael Deilmann for the O_2 permeation measurements. This project is supported by the German science foundation in the coordinated research center SFB 591.

References

[1] Becker K, Schoenbach K and Eden J 2006 *J. Phys. D: Appl. Phys.* **39** R55
[2] Foest R, Schmidt M and Becker K 2006 *Int. J. Mass Spectrom.* **248** 87
[3] El-Habachi A, Shi W, Moselhy M, Stark R H and Schoenbach K H 2000 *J. Appl. Phys.* **88** 3220
[4] Eden J G, Park S-J, Ostrom N P and Chen K-F 2005 *J. Phys. D: Appl. Phys.* **38** 1644
[5] Franzke J, Kunze K, Miclea M and Niemax K 2003 *J. Anal. At. Spectrom.* **16** 802
[6] Rahul R *et al* 2005 *J. Phys. D: Appl. Phys.* **38** 1750
[7] Ichiki T, Tauro R and Horiike Y 2004 *J. Appl. Phys.* **95** 35
[8] Sankaran R M and Giapis K P 2003 *J. Phys. D: Appl. Phys.* **36** 2914
[9] Shimizu Y, Sasaki T, Ito T, Terashima K and Koshizaki N 2003 *J. Phys. D: Appl. Phys.* **36** 2940
[10] Kikuchi T, Hasegawa Y and Shirai H 2004 *J. Phys. D: Appl. Phys.* **37** 1537
[11] Léveillé V and Coulombe S 2005 *Plasma Sources Sci. Technol.* **14** 467
[12] Moravej M, Yang X, Nowling G R, Chang J P and Hicks R F 2004 *J. Appl. Phys.* **96** 7011
[13] Yanguas-Gil A, Focke K, Benedikt J and von Keudell A 2007 *J. Appl. Phys.* **101** 103307
[14] Benedikt J, Focke K, Yanguas-Gil A and von Keudell A 2006 *Appl. Phys. Lett.* **89** 251504
[15] Niemi K, von der Gathen V S and Döbelle H F 2005 *Plasma Sources Sci. Technol.* **14** 375
[16] Yang X, Moravej M, Nowling G R, Babayan S E, Panelon J, Chang J and Hicks R 2005 *Plasma Sources Sci. Technol.* **14** 314
[17] Capitelli M, Ferreira C, Gordiets B and Osipov A 2000 *Plasma Kinetics in Atmospheric Gases* 1st edn (Berlin: Springer)
[18] Park J, Henins I, Herrmann H W, Selwyn G S and Hicks R F 2001 *J. Appl. Phys.* **89** 20
[19] Brok W J M, Bowden M D, van Dijk J, van der Mullen J J A M and Kroesen G M W 2005 *J. Appl. Phys.* **98** 013302
[20] van Hest M F A M, Klaver A, Schram D C and van de Sanden M C M 2004 *This Solid Films* **449** 40
[21] Chou J S and Lee S C 1995 *J. Appl. Phys.* **77** 1805
[22] Nowling G R, Yajima M, Babayan S E, Moravej M, Yang X, Hoffman W and Hicks R F 2005 *Plasma Sources Sci. Technol.* **14** 477
[23] Creatore M, Cigal J-C, Kroesen G and van de Sanden M 2005 *Thin Solid Films* **484**104
[24] Babayan S E, Jeong J Y, Schütze A, Tu V J, Moravej M, Selwyn G and Hicks R 2001 *Plasma Sources Sci. Technol.* **10** 573